

Rapid mechanochemical synthesis of nickel-vanadium carbide nanocomposite by magnesiothermic reaction

Danial Davoodi^{a, b, *}, Amir Hossein Emami^c, Morteza Tayebi^d, Seyed Kamal Hosseini^c

^a Young Researchers and Elite Club, Najafabad Branch, Islamic Azad University, Najafabad, Isfahan, Iran

^b Kherad Sanat Arvand Company, Research and Development Unit, Engineering Department, Khorramshahr, Iran

^c Advanced Materials Research Center, Materials Engineering Department, Najafabad Branch, Islamic Azad University, Najafabad, Iran

^d Young Researchers and Elites Club, Science and Research Branch, Islamic Azad University, Tehran, Iran

ARTICLE INFO

Keywords:

Ni-VC nanocomposites
Mechanochemical synthesis
High energy ball milling
Williamson-Hall equation
Magnesiothermic reaction

ABSTRACT

In the present study, in-situ production of Ni-VC nanocomposite powder synthesized from several raw materials including NiO, V₂O₅, Mg and C, was carried out through mechanochemical approach by means of magnesiothermic reaction. Due to high adiabatic temperature ($T = 3964$ K), this reaction is known as a self-propagating reaction or MSR. Raw materials were mixed at 1:1:6:2 stoichiometric ratios of nickel oxide, vanadium oxide, magnesium and graphite, respectively. Milling process was carried out in a high-energy planetary ball mill under argon atmosphere with various ball-to-powder weight ratios (15:1, 20:1 and 25:1) for the aim of obtaining the optimum ball-to-powder weight ratio to reduce the synthesis time. After milling for 30 min and 40 min, combustion occurred in the milling vial for 25:1 and 20:1 ball-to-powder weight ratios, respectively. The microscopic properties of milled nanocomposite powders were investigated by X-ray diffraction (XRD), field emission scanning electron microscopy (FE-SEM) and transmission electron microscopy (TEM). According to XRD patterns, after combustion reaction, anticipated products including nickel, vanadium carbide (VC) and magnesium oxide (MgO) were totally produced. To remove undesirable MgO phase, leaching process (1 M HCl at 80 °C for 1 h) was used. According to XRD and X-ray-mapping analyses before and after the leaching process, HCl dissolved MgO phase thoroughly. Additionally, crystallite size and lattice strain were calculated based on Williamson-Hall method; these values were calculated 54 nm and 0.00615 for VC, while they were 40 nm and 0.00595 for nickel, respectively. Moreover, according to TEM micrograph, the morphology of the particles after leaching process was found to be spherical with the size of 50 ± 5 nm.

1. Introduction

By considering the high hardness, abrasion resistance, thermal and chemical stability, thermal shock resistance and high corrosion resistance properties, researchers have recently focused on development and improvement of cermets. Chemical and physical stability of cermets make them ideal to be used as cutting tools, forming tools and wear resistant components such as drilling coverings and molds [1]. Since typical cermets mostly contain a carbide phase and metal binder, nickel is conventionally used as a metallic binder [2]. This is because Ni has a good wettability with carbide-reinforcement particles [3] and can be used as a binder to increase the nanocomposite toughness. In this sense, with the presence of a hard phase (carbide) and a soft phase

such as Ni, both high hardness and toughness properties are introduced to the composite. While several studies have been carried out on cermets with a variety of carbide systems such as NbC, WC, TaC, ZrC, HfC, TiCN, etc., few have been done on nickel matrix and VC reinforcement [3–8].

One of the most widely used techniques to manufacture cermets is self-propagating high-temperature synthesis, which has developed most of the current advanced materials. The process of self-propagating high-temperature synthesis can be divided into three basic stages: (i) ignition, (ii) combustion wave passing through and (iii) product cooling. Combustion synthesis is a method based on thermal properties of some exothermic reactions in which a significant amount of heat is generated through reaction of small amounts of raw materials. The generated heat can provide the activation energy required for the adjacent unreacted layers of raw materials, and therefore the reaction prop-

* Corresponding author at: Young Researchers and Elite Club, Najafabad Branch, Islamic Azad University, Najafabad, Isfahan, Iran.

Email addresses: Davoodi.danial@smt.iaun.ac.ir, Davoodi.danial80@gmail.com (D. Davoodi); Dr.s.a.h.emami@gmail.com (A.H. Emami); Mortezatayebi95@yahoo.com (M. Tayebi); Kamalhosseini23@yahoo.com (S.K. Hosseini)

agates to the other parts as well. The final products are produced when the reaction is completed for the whole sample. The advantages of combustion synthesis approach are simplicity, cost-effectiveness, time-effectiveness, high purity of the products and possibility of simultaneous formation of the cermet [9–12]. Also, it is shown that cermets produced by solid-state sintering approach have superior properties than those prepared by conventional methods. Since in most conventional methods, a heat treatment step is imposed on the material, grain growth is inevitable. On the other hand, physical and mechanical properties of the material are directly dependent on the grain size, i.e. the smaller the size of the grain, the more desirable mechanical properties are [13]. In the meantime, it is possible to produce a variety of advanced materials, including carbides [13], nitrides [14], borides [15], and nanocomposites [16] in the shortest possible time by means of mechanochemical method [17]. This method is coupled with the milling process and gives rise to grain fineness in the minimum production time that provides the optimum conditions for mechanical properties. To our best knowledge, no study has been so far carried out on in-situ synthesis of Ni-VC nanocomposites. For this purpose, the synthesis of VC was investigated separately. VC synthesis has been done by different techniques such as direct reaction of components [18], reaction at specific temperatures [19,20], reduction by gas carbonization [21,22], mechanical alloying [23], salt-bath electrolysis, chemical deposition and chemical vapor deposition (CVD) [24]. VC was first synthesized by heating V_2O_5 and sugar charcoal in the absence of air. In other methods, reaction of vanadium hydride and carbon is carried out in 2000 °C under reductive atmosphere. However, these methods demand high temperature and are not cost-effective [24].

Attempts were already made to synthesize VC at the lowest possible temperature and minimum time. Zhang and Li [18] reduced V_2O_5 in the presence of Mg and carbon and synthesized VC after 36 h of milling. Nikolaenko et al. [25] investigated the synthesis of VC powder by heating and using two methods: by liquid phase deposition with a furnace at temperature range of 1100–1200 °C under argon atmosphere, and at low temperature by microwave method with V_2O_5 , NH_4OH and carbon as precursors; which V_8C_7 was obtained after drying the materials at 120 °C. Mahajan et al. [26,27] used V_2O_5 , Mg, and acetone as a carbon source for synthesis of VC nanoparticles. The process was completed by heating the materials in a furnace for 5 h and 18 h at 800 °C. As a result, synthesis reaction occurred and VC was generated. Liu et al. [28] employed NH_4VO_3 precursor for synthesis of VC nanoparticles and results showed that VC nanoparticles were synthesized after a heat treatment process at 900 °C for 1 h. In a similar attempt, Zhao et al. [29] used NH_4VO_3 precursor with carbon in an aqueous solution where they obtained V_8C_7 at 150 °C after drying. Elsewhere, Hassanzadeh-Tabrizi et al. [30] produced VC nanopowder by MSR type of mechanochemical approach in a time period of 80 min. The investigation was in parallel with a previous study [31] where synthesis took as long as 1440 min. In the above-mentioned studies, a number of difficulties were reported including agglomeration, inappropriate distribution, impurities, and non-reacted precursors. All in all, it is clear that methods employed in previous research requires high temperature, long time and high cost.

The main purpose of this research, however, is to produce Ni-VC nanopowder composite by means of in-situ mechanochemical synthesis from raw oxide materials at ambient temperature without an expensive heat treatment. Also, in this study, ball-to-powder weight ratio was examined as a milling parameter affecting the synthesis time.

2. Materials and methods

2.1. Raw materials

All materials including NiO (99.5%, < 200 μ m), V_2O_5 (99.7%, 250 μ m), Mg (99.8%, < 400 μ m) and graphite (% 95, < 0.3 μ m) were

obtained from Merck Co. and used as-received to produce Ni-VC nanocomposite powder.

2.2. Nanocomposite synthesis

In order to perform in-situ production of Ni-VC nanocomposite, a powder mixture of NiO, V_2O_5 , Mg and graphite at 1:1:6:2 M ratios was milled by different time intervals, respectively. The ball mill process was performed in a planetary ball mill (FP model X200, Iran) with ball-to-powder weight ratios of 15:1, 20:1, 25:1 at 600 rpm under 99.99% pure argon atmosphere and 6.5 gr powder for all ball-to-powder weight ratios. In every step of the ball milling process, the produced powder was analyzed by XRD to assess the phase transformation during the process. Then, HCl 1 M solution was used to remove MgO phase at 80 °C for 1 h [32].

2.3. Characterization

X-ray diffraction device (Philips model PW3040, Netherlands) was used for phase analysis in the range of $2\theta = 10-90^\circ$ and 0.05° step size in voltage of 30 kW and current of 30 mA. In all experiments, X-ray $CuK\alpha$ monochromatic wavelength ($\lambda = 1.5405 \text{ \AA}$) was employed. To identify the phases, X'Pert HighScore software was employed. Examination of powder particles was carried out by FE-SEM (Cam Scan model MV2300), energy dispersive spectroscopy (EDS) analysis, mapping analysis and TEM under accelerating voltage of 120 kV (Philips model CM120, Netherlands) to investigate the morphology and determine the particle size of nanocomposite samples.

2.4. Thermodynamic calculations

In order to evaluate the thermodynamic behavior and calculate free energies, the enthalpy of formation and the adiabatic temperature of the reactions, HSC Chemistry software version 5 and Eq. (1) [33] were utilized.

$$\begin{aligned} \Delta Q &= -\Delta H_{298}^\circ + \int_{298}^{T_m} \sum C_p(\text{Solid}) .dT \\ &+ \Delta H_m + \int_{T_m}^{T_{ad}} \sum C_p(\text{Liquid}) .dT \\ &= 0 \end{aligned} \quad (1)$$

where C_p , ΔH_{298}° and ΔQ are specific heat capacity, standard enthalpy changes of formation at 298 K and heat of reaction, respectively. When the adiabatic temperature gets higher, the self-propagating high-temperature reaction possibility increases as well. The total released heat by a process is usually a thermodynamic driving force for the process itself. For a self-propagating combustion process to be done, the released heat must be more than the heat given to the surrounding.

2.5. Crystallite size and lattice strain calculations

The Williamson-Hall equation (Eq. (2)) was used to obtain the size of the crystallites as well as the lattice strain of the Ni-VC composite; details are given in [34].

$$\beta \cos \theta = \frac{0.98\lambda}{d} + 2A\epsilon \sin \theta \quad (2)$$

In this equation, β is the full width at half maximum (FWHM) of the Bragg peak, d is the crystallite size, λ is the X-ray wavelength, θ is the diffraction angle and ϵ is the lattice strain.

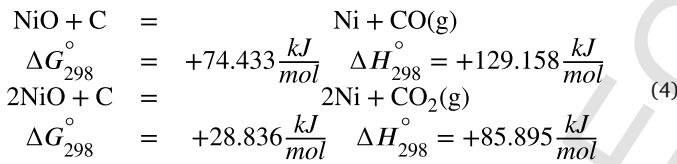
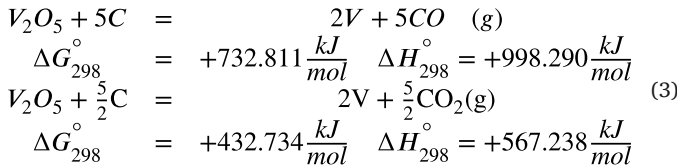
3. Results and discussion

3.1. Thermodynamic aspects of reactions

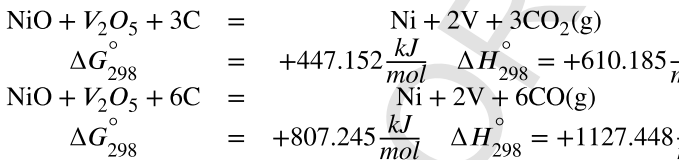
To further investigate the thermodynamic behavior of possible reactions, the possibility of each reaction was first determined and then relative diagrams were plotted for different temperatures. Also, in order to predict the gradual or instant type of mechanism of the process, theoretical adiabatic temperature of the reactions was calculated using thermodynamic data to predict the type of reaction in milling vial. The theoretical process of the Ni-VC nanocomposite production by the mechanochemical process of raw oxide materials can be divided into following steps. It is worth noting that all these steps practically took place in a few seconds after the combustion occurred in the milling vial.

3.1.1. Investigation of the reduction system by carbothermic reactions

In presence of graphite as a reducing agent, reduction of V_2O_5 and NiO phases is very unlikely to occur. Therefore, the standard enthalpy and Gibbs free energy data presented in reactions (3) and (4) show that this reaction is endothermic. Moreover, the possibility of its occurrence is unpredictable.

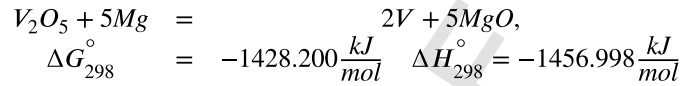
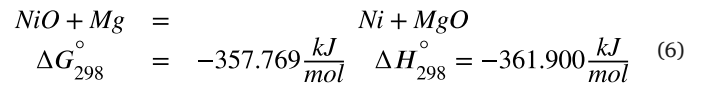


According to thermodynamic data presented in reaction (5), an highly endothermic reaction was observed in the triple system of V_2O_5 , NiO and graphite; and similar conditions were seen for binary reactions.



3.1.2. Reduction system by magnesiothermic reaction

In the presence of Mg, reduction of NiO (reaction (6)) and V_2O_5 (reaction (7)) are highly exothermic reactions mostly due to the negative free energy and negative enthalpy. Thermodynamically, the reactants are susceptible to be reduced during milling process. Both reactions result in release of 361,900 J/mol and 1,456,998 J/mol heat, while the calculated adiabatic temperatures are 3106 and 4188 K, respectively. Moreover, this indicates that the reaction is a self-propagating high-temperature.

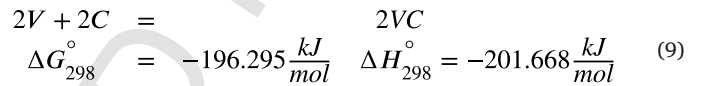


Given the thermodynamic prediction of the presence of NiO, V_2O_5 and Mg in reaction (8), given the negative enthalpy, the negative free energy and adiabatic temperature of 3861 K, it is clear that conditions similar to binary reactions occur and both reactants can act as reductant, too.

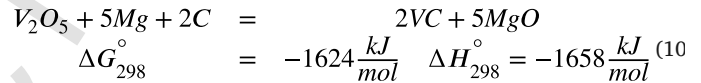


In fact, according to thermodynamic calculations, Mg acts as the reducing agent and reduces both NiO and V_2O_5 phases.

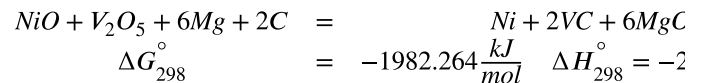
In the next step (reaction (9)), vanadium is reduced during the milling and produces VC phase. This reaction leads to release of 201668 J/mol heat with an adiabatic temperature of 2214 K.



Nickel acts as a metallic base in nanocomposite and shows no carbide production in the presence of vanadium due to its poor tendency to form carbide. Hence, the reaction of carbide vanadium production (reaction (10)) leads to a release of 1,658,000 J/mol heat and an adiabatic temperature of 4341 K.



Finally, the general form of Ni-VC composite reaction is given as reaction (11) accompanied by the release of 2,020,566 J/mol heat and an adiabatic temperature of 3964 K.



The adiabatic temperature of chemical reactions exceeds the critical value (1800 K). Therefore, these chemical reactions seem to progress as self-propagating high-temperature mechanically-induced reaction (MSR) [35]. So it is necessary that the initial activation energy to be supplied by either thermal or mechanical sources. On the other hand, considering the high energy ($\Delta H_{298}^\circ = -2,020,566$ J/mol) released by reaction (11), it is predicted that the chemical reaction occurs along with a combustion in milling vial.

Figs. 1 and 2 illustrate the standard enthalpy changes and free energy of formation of reactions of this system, respectively. According to these diagrams, the standard enthalpy changes of formation and free energy of reactions lie in the negative part of the diagram implying possibility of the reactions ($\Delta G < 0$) and highly exothermic status of the reactions ($\Delta H < 0$). Besides, the in-situ production of Ni-VC nanocomposite (reaction (8)) is located in the negative side of the graph. For this reason, this reaction holds a more appropriate condition and higher priority than the other two reactions.

Considering the above-mentioned reactions and calculations, it is evident that all magnesiothermic reactions are exothermic and thermodynamically possible, but the carbothermic reactions are endothermic.

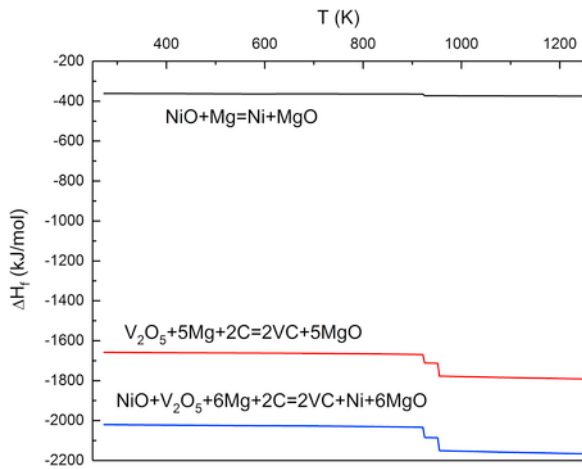


Fig. 1. Changes in formation heat vs. temperature variations.

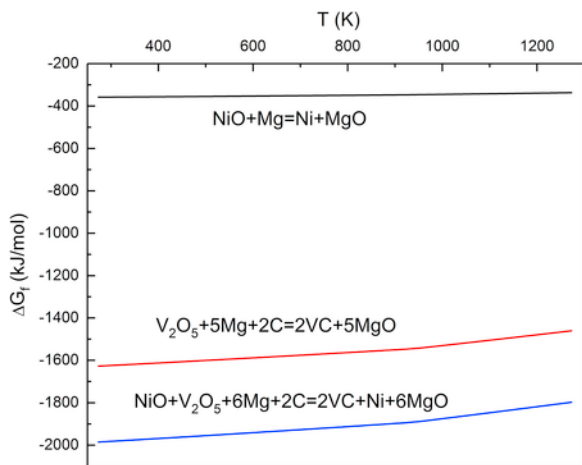


Fig. 2. Free energy vs. temperature variations.

3.2. The effect of ball-to-powder weight ratio

Since the mechanical activation is a complex process, it is significant to optimize the affecting factors on the process in order to prepare the phase or the desired structure in the shortest possible time. In this study, effect of ball-to-powder weight ratio on in-situ production of Ni-VC nanocomposite was examined to obtain the optimum weight ratio of ball-to-powder during synthesis time.

Figs. 3–5 represent the XRD patterns of raw materials powder mixture at different time intervals of the milling process for ball-to-powder weight ratios of 15:1, 20:1 and 25:1, respectively. As it is evident, for the specimen with the ball-to-powder weight ratio of 15:1 (Fig. 3), the milling is kept on for 120 min and neither combustion occurs during this time, nor displacement reaction occurs between oxide materials (NiO, V₂O₅). Similarly no reduction agents (Mg, C) are generated. This suggests that 15:1 ball-to-powder weight ratio failed to provide the required energy for mechanical activation. In this case, more time should be spent on milling process or an additional operation such as heat treatment is required. Nevertheless, the combustion reaction occurs in milling vial after 40 min and 30 min with the weight ratio of ball-to-powder 20:1 and 25:1, respectively.

The reduction of reaction time from 40 min to 30 min for the sample with 25:1 ball-to-powder weight ratio compared to the one with 1:20 ratio can be attributed to the amount of extra-generated energy. This results in the production of composite in shorter time (30 min milling). Besides, results of previous studies [36] demonstrated that the

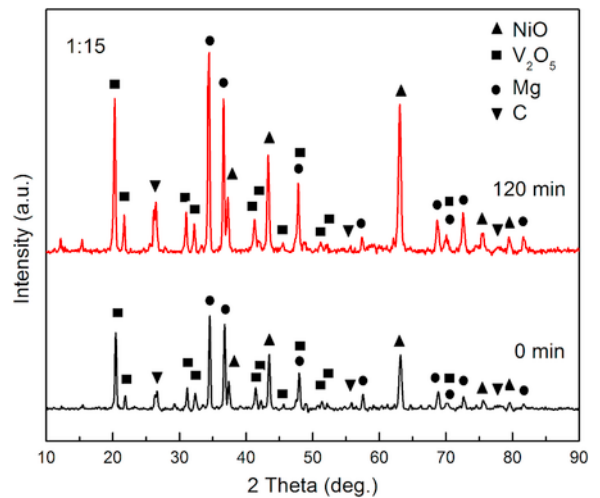


Fig. 3. XRD patterns of NiO, V₂O₅, Mg and C powder mixture which was milled at different milling times with 15:1 ball-to-powder weight ratio.

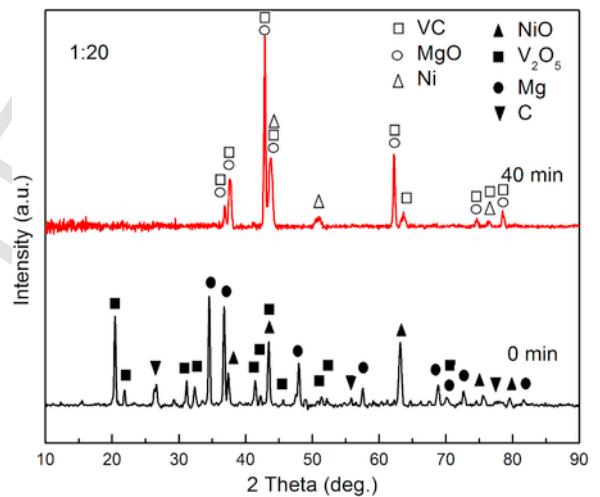


Fig. 4. XRD patterns of NiO, V₂O₅, Mg and C powder mixture which was milled at different milling times with 20:1 ball-to-powder weight ratio.

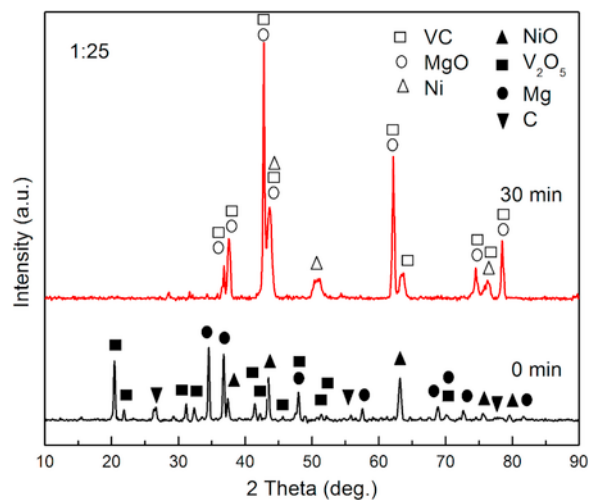


Fig. 5. XRD patterns of NiO, V₂O₅, Mg and C powder mixture which was milled at different milling times with 25:1 ball-to-powder weight ratio.

size of crystallites and the time required for the formation of phases decreased with increasing the ball-to-powder weight ratio, possibly because the impact energy between the balls and the balls-vial collisions increases by increasing the weight of the balls. Similarly, the required time for reduction and formation of phases is significantly affected by growth per collision.

It is in accordance with the formulation of the specific work W_T (grinding energy divided by the mass of the material that is being ground) a planetary ball mill:

$$W_T = \frac{m_1}{m_2} b n \tau D \quad (12)$$

where m_1 , m_2 , b , n , τ and D are the mass of grinding media, the mass of material charge, acceleration, speed, grinding time and drum diameter, respectively [37]. It is clear that for a specific amount of W_T , increasing in $\frac{m_1}{m_2}$ caused to decrease the necessary grinding time.

3.3. Survey of phase transformations

Fig. 6 shows XRD pattern of raw materials before milling. Regarding the pattern, no product is produced within the first 20 min of the reaction and the raw materials remained as oxides. However, only due to milling process, the intensity of the peaks reduces and the width of the peaks increases.

In order to investigate this in more details, the main two peaks of V_2O_5 phase were carefully examined at time intervals of 0 and 20 min (Fig. 7). As it can be seen, after 20 min milling, intensity of the peaks decreased and peak was broadened. During the milling process, the density of crystallographic defects in the structure increases due to frequent contact of the balls with powder particles which is mainly due to plastic deformation and cold-working. These defects can include dislocations, vacancies, and grain boundaries [38,39]. Increase of dislocations causes these imperfections to be locked in each other and the so-called powder became strain hardened. Therefore, this event results in grain boundary fracture due to collision of balls with powder particles, reducing the crystallite size and creating new surfaces.

In fact, the occurrence of mechanical operation in the powder results in high density of dislocation in powder particles. The raise of dislocation density other crystallographic defects remove atoms from their random position in the crystal lattice; therefore, the crystal lattice would have an elastic deformation and the space between their atomic planes would be changed. Hence, a distinctive crystalline plane with

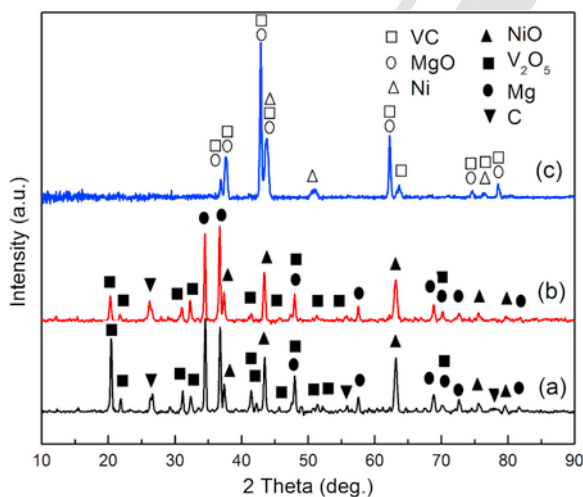


Fig. 6. XRD patterns of NiO, V_2O_5 , Mg and C powder mixture which was milled with 25:1 ball-to-powder weight ratio at: (a) 0 min, (b) 20 min, and (c) 30 min.

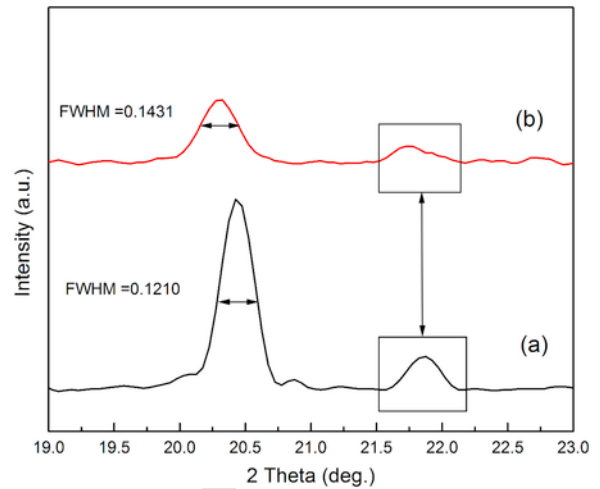


Fig. 7. Changes in the initial peaks intensity of V_2O_5 at: (a) 0 min and (b) 20 min.

different diffraction angles, close to each other, can be applied in Bragg's law. Additionally, peaks close to each other for a given plane turn out to be a broad peak. Reduction in the crystallite size is a key factor that leads to broadening of the peaks.

When the grains become finer, the number of crystalline planes in the grain decreases. In other words, the number of planes that should make constructive interference decreases and Bragg's angles are not removed. Hence, Bragg's angles would be diffracted too and so a broad peak would appear [39].

By increasing the milling time, new interfaces are continuously produced. As a result, the interface between Mg (reduction agent) and the initial oxide materials (V_2O_5 , NiO) increases. All defects caused by milling process are responsible for formation of new interfaces in the structure and shortened the diffusion paths [38,39]. Atoms in the interfaces deviate from the equilibrium state and make use of energy to destabilize the atoms balance, so the atoms interfaces keep a higher energy level. Thermodynamically, each system tends to reach the lowest possible energy level. The displacement reaction between oxides (V_2O_5 , NiO) and the reducing agent (Mg) occurs due to favorable reduction conditions with respect to presence of Mg in the system in 30-min milling time. High amount of energy released from the combustion process causes the combustion in the vial to reduce the adjacent particles in the shortest amount of time. Likewise, the heat released from NiO and V_2O_5 reduction reactions provides the activation energy required for reaction between V and C. Also, VC phase would be produced in accordance with reaction (7).

3.4. Individual examination of NiO-Mg and V_2O_5 -Mg-C systems

According to the previous study [30], VC was mechanochemically synthesized in a reaction time of 80 min individually (based on reaction 10). Also, Fig. 8 indicates XRD patterns in 0 min and 8 min time intervals for nickel alloy production system. In this system, combustion reaction occurs in the combustion vial within 8 min after the beginning of milling process that results in the production of nickel alloy and MgO. Firstly, it can be concluded that although thermodynamically, the possibility of VC production was higher than metallic nickel production and the kinetics of this reaction was much faster (8 min). Secondly, in in-situ production system of Ni-VC composites, the start of the combustion reaction was induced by reduction of NiO particles and the combustion wave of these particles led to reduction of other adjacent particles, i.e., V_2O_5 , which caused the reaction to take place completely within 30 min.

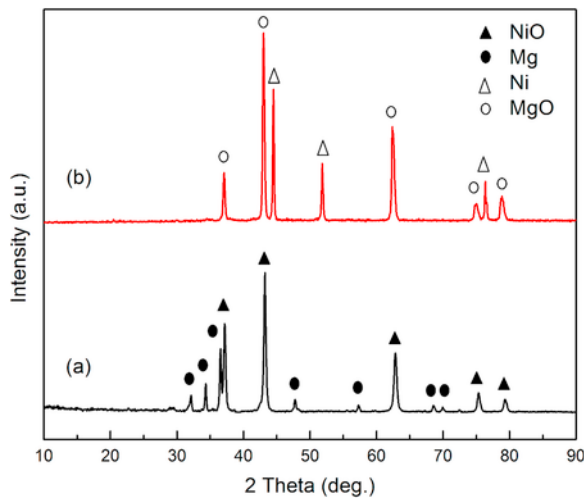


Fig. 8. XRD patterns of transformation in NiO-Mg system: (a) before milling, (b) after the combustion (8 min milling).

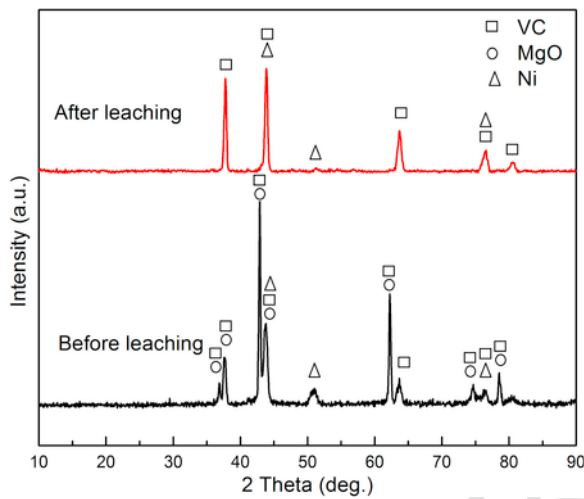


Fig. 9. XRD patterns after 30 min of milling, before and after leaching.

3.5. Elimination of MgO phase in NiO-V₂O₅-Mg-C system

Fig. 9 shows the XRD patterns before and after the leaching process. It indicates that MgO phase was completely removed during leaching process, emphasizing that HCl dissolved MgO phase entirely and the process was successful. Finally, with respect to XRD patterns, Ni-VC nanocomposite powder remained in the system after leaching process. Mapping analysis was used to verify the results of our study.

Fig. 10 illustrates the X-ray mapping of the synthesized powder before leaching. Accordingly, analysis of X-ray mapping shows the presence of MgO, nickel and VC phases, which represents the Ductile-Brittle system after milling. It is clear that particle agglomeration occurred too. A major drawback of material production through mechanochemical method is entrance of contaminations and impurities, such as iron, due to frequent collisions of the balls with the walls of the milling vial with increasing milling time. EDS analysis was performed before and after the leaching process in order to determine the impurity contamination of the synthesized powder. EDS analysis both before and after leaching process shows that the balls and the mill walls did not introduce any impurities, such as iron, to the synthesized powder.

Fig. 11 shows the FE-SEM micrograph and X-ray mapping analysis of the synthesized powder after leaching process. EDS analysis reveals that MgO phase was completely eliminated, which is consistent with the results of XRD patterns. Thus, it is obvious that leaching process is successfully performed. Similarly, the mapping analysis reveals that VC reinforcement particles were uniformly distributed in nickel matrix both before and after leaching process. Therefore, this can be considered as one of the main advantages of in-situ mechanochemical nanocomposite production.

3.6. Morphology evaluation of Ni-VC nanocomposite

Figs. 12 and 13 present FE-SEM micrographs of nanocomposite powder before and after leaching process at different magnifications. The production reaction of Ni-VC nanocomposite was extremely exothermic and accompanied by combustion. This released heat and combustion caused melting of particles' surfaces and made the particles bond together. This can be seen thoroughly before the leaching process (Fig. 12). However, the particle fusion was removed due to complete dissolution of MgO phase in HCl. In addition, the particle agglomeration can be easily observed in images obtained after leaching process.

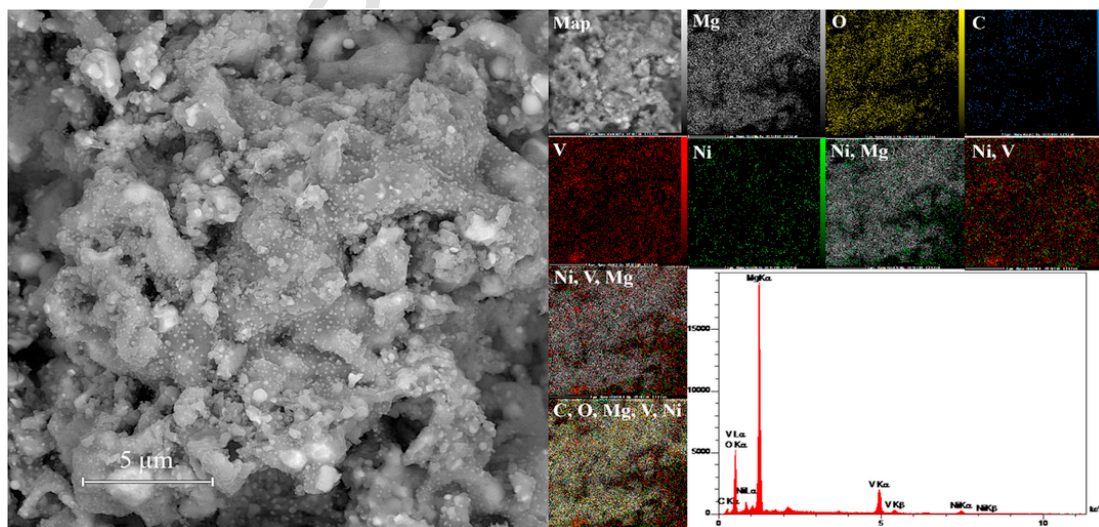


Fig. 10. X-ray mapping analysis and EDS analysis before the leaching process.

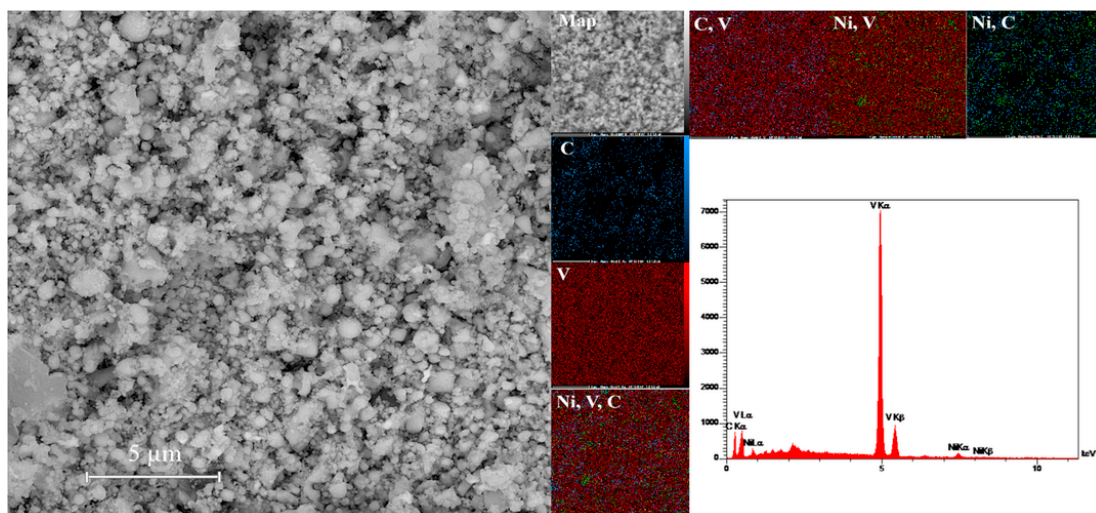


Fig. 11. X-ray mapping analysis and EDS analysis after the leaching process.

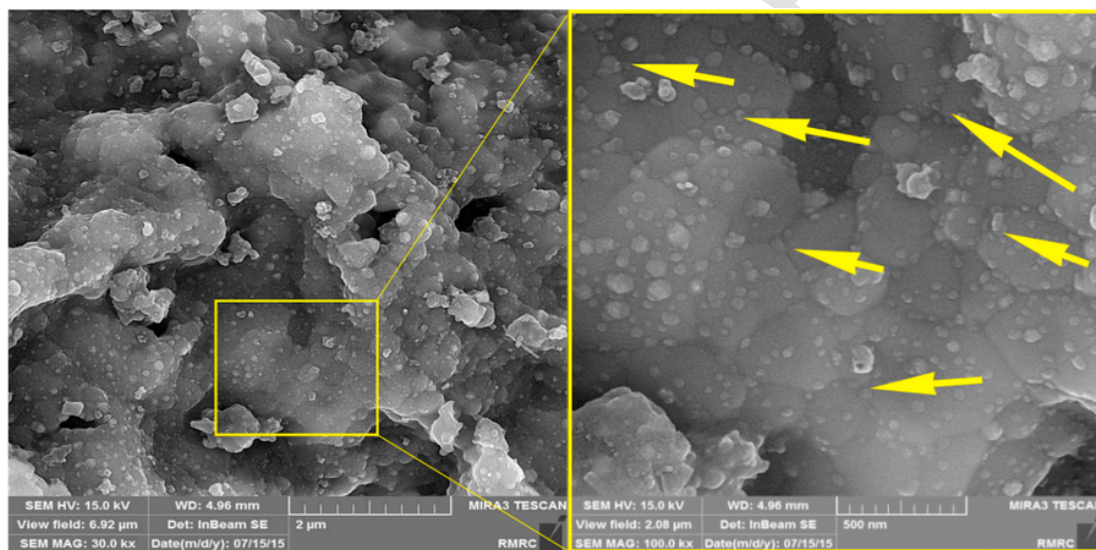


Fig. 12. FE-SEM micrographs of the powder particles before the leaching process. (Yellow arrows in the Fig. represent the fused areas due to combustion).

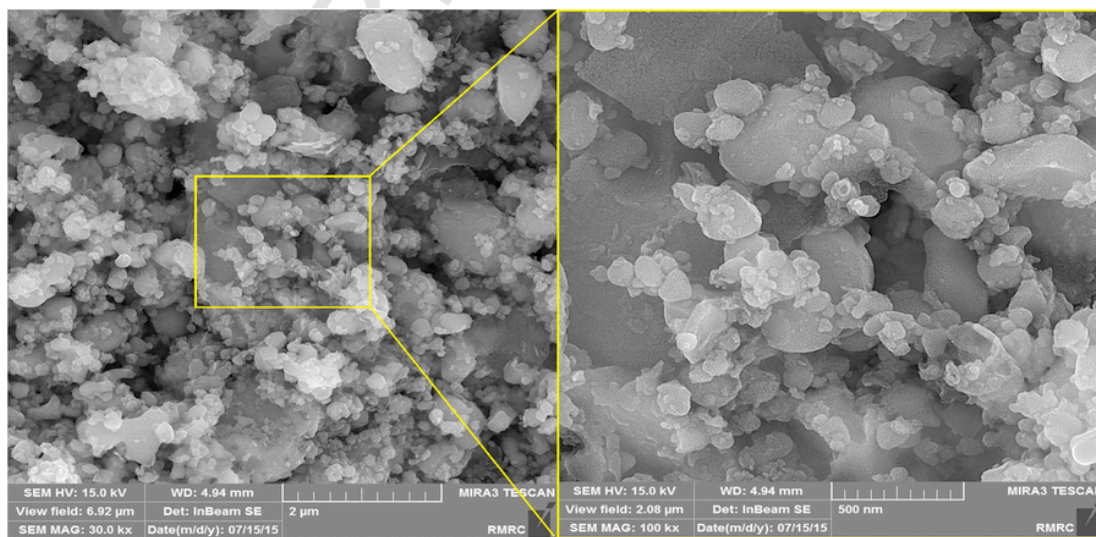


Fig. 13. FE-SEM micrographs after the leaching process.

Each system tends to reduce its energy level, this can be achieved by agglomeration process, thus, tending to reduce the specific surface area of particles which can intensify the agglomeration process and thermodynamically increase the level of the free energy [40]. According to FE-SEM images, it can be said that the size of these particles reduced to values lower than 100 nm after leaching process which confirms the nanoscale structure of these agglomerates.

3.7. Calculation of crystallite size of NiO-V₂O₅-C-Mg system

Fig. 9 depicts XRD pattern of Ni-VC nanocomposite powder after leaching process. To obtain crystallite size using Williamson-Hall relation, the $\beta\cos\theta$ data was calculated with respect to $\sin\theta$ and was plotted for different peaks of nickel and VC according to Figs. 14 and 15. Then, lattice strain and crystallite size were calculated from the slope and y-intercept of the fitted line, respectively. Hence, the crystallite size and lattice strain for VC were 54 nm and 0.00615 while for nickel they were 40 nm and 0.00595, respectively.

Fig. 16 represents TEM micrograph of nanocomposite powder after leaching process. According to the image, it can be said that the particles morphology was semi-spherical. Similarly, the average particle size was 55 ± 5 nm, which confirmed the calculations of Williamson-Hall equation and highlighted the nanoscale structure of the produced composite powder.

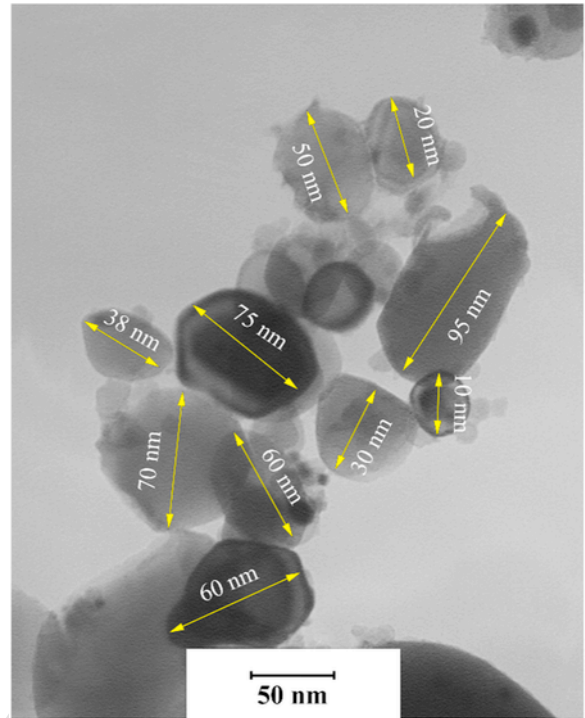


Fig. 16. TEM micrograph of nanocomposite powder after leaching.

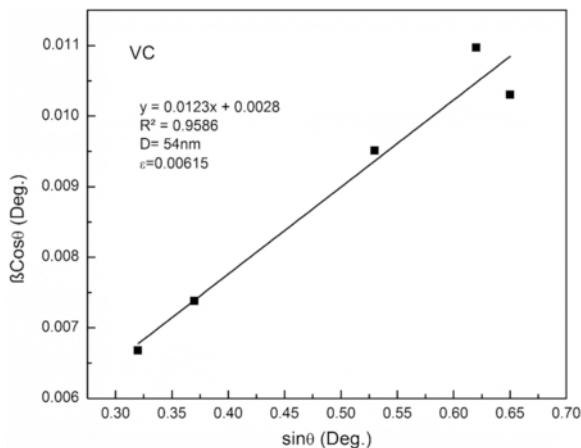


Fig. 14. $\beta\cos\theta$ vs. $\sin\theta$ diagram for VC powder.

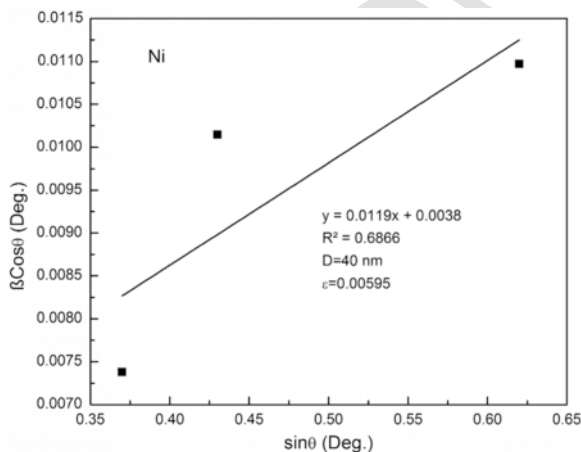


Fig. 15. $\beta\cos\theta$ vs. $\sin\theta$ diagram for nickel powder.

4. Conclusions

In summary, the purpose of this study was to prepare Ni-VC nanocomposite powder from NiO, V₂O₅, Mg and C through mechanochemical approach by means of magnesiothermic reaction without a costly heat treatment.

The results of this research are summarized as follows:

- i) Due to thermodynamic behavior of Ni-VC nanocomposite production, MSR reaction was found to be suitable for reduction process. With regard to adiabatic temperature (3964 K), the reaction proceeded as a self-propagating high-temperature synthesis. So, due to the large amount of released heat ($-2,020,566$ J/mol), this reaction is accompanied by combustion.
- ii) With increasing the ball-to-powder weight ratio, the required time for nanocomposite synthesis decreased, which was due to high generated energy released from the balls collision to the particle surfaces.
- iii) Ni-VC nanocomposite powder was successfully synthesized via mechanochemical approach within 30 min of milling. According to microscopic evaluation and EDS analyses, no impurities like iron entered from balls or vial walls during milling process.
- iv) According to XRD patterns and X-ray mappings of nanocomposite powder both before and after the leaching process, MgO which was a byproduct of this reaction was completely removed from nanocomposite powder by 1 M HCl within 60 min at the temperature of 80 °C.
- v) The crystallite size and the lattice strain of the nickel and VC powder were calculated using Williamson-Hall equation after leaching process. Eventually, the average crystallite sizes of 40 and 54 nm, and the lattice strain of 0.00595 and 0.00615 were reported for nickel powder and VC, respectively.
- vi) According to TEM micrograph, the particle size was about 55 ± 5 nm, which confirmed the calculated crystallite size through

Williamson-Hall relation. Also, the particles morphology was semi-spherical.

- vii) According to FE-SEM images after combustion, due to released heat, the surfaces of the particles were partially melted and particle fusion was occurred. Whereas, after leaching process, due to removal of MgO phase, particles were separated from each other. Again high free surface of particles led to agglomeration.

References

- [1] B. Liu, S. Huang, J.V. Humbeeck, J. Vleugels, Influence of HfH_2 addition on the microstructure and mechanical properties of TiC-NiTi cermets, *Mater. Des.* (2017) <https://doi.org/10.1016/j.matdes.2017.07.044>.
- [2] P. Ettmayer, W. Lengauer, The story of cermets, *Int. J. Powder Metall.* 21 (1989) 37–38.
- [3] V. Verma, B.V. Manoj Kumar, Sliding wear behavior of SPS processed TaC-containing Ti(CN)-WC-Ni/Co cermets against silicon carbide, *Wear* 376–377 (2017) 1570–1579.
- [4] S.G. Huang, J. Vleugels, H. Mohrbacher, M. Woydt, Microstructure and mechanical properties of NbC matrix cermets using Ni containing metal binder, *Met. Powder Rep.* (2016) <https://doi.org/10.1016/j.mprp.2016.05.009>.
- [5] K. Mandel, M. Radajewski, L. Krüger, Strain-rate dependence of the compressive strength of WC-Co hard metals, *Mater. Sci. Eng. A* 612 (2014) 115–122.
- [6] P. Siwak, D. Garbiec, Microstructure and mechanical properties of WC-Co, WC-Co-Cr₃C₂ and WC-Co-TaC cermets fabricated by spark plasma sintering, *Trans. Nonferrous Met. Soc. China* 26 (2016) 2641–2646.
- [7] J. Lee, J. Kim, S. Kang, Advanced W-HfC cermet using in-situ powder and spark plasma sintering, *J. Alloy. Compd.* 552 (2013) 14–19.
- [8] D. Yung, A. Zikin, I. Hussainova, H. Danninger, E. Badisch, A. Gavrilovic, Tribological performances of ZrC-Ni and TiC-Ni cermet reinforced PTA hardfacings at elevated temperatures, *Surf. Coat. Technol.* 309 (2017) 497–505.
- [9] P. Mossino, Some aspects in self-propagating high-temperature synthesis, *Ceram. Int.* 30 (2004) 311–332.
- [10] K.C. Patil, S.T. Aruna, T. Mimani, Combustion synthesis: an update, *Curr. Opin. Solid State Mater. Sci.* 6 (2002) 507–512.
- [11] M.J. Capaldi, A. Saidi, J.V. Wood, Reaction synthesis of TiC and Fe-TiC composites, *ISIJ Int.* 37 (1997) 188–193.
- [12] M.S. Song, B. Huang, M.X. Zhang, J.G. Li, Study of formation behavior of TiC ceramic obtained by self-propagating high-temperature synthesis from Al-Ti-C elemental powders, *Int. J. Refract. Met. Hard Mater.* 27 (2009) 584–589.
- [13] D. Davoodi, S.A. Hassanzadeh-Tabrizi, A.H. Emami, S. Salahshour, A low temperature mechanochemical synthesis of nanostructured ZrC powder by a magnesiothermic reaction, *Ceram. Int.* 41 (2015) 8397–8401.
- [14] D.P. Thompson, Mechanochemical nitride synthesis, *Mater. Sci. Forum* 554 (2007) 51–57.
- [15] K. Izumi, K. Kudaka, D. Maezawa, T. Sasaki, Mechanochemical synthesis of chromium borides, *J. Ceram. Soc. Jpn.* 107 (1999) 491–493.
- [16] S.A. Hassanzadeh-Tabrizi, H. Hosseini Badr, S. Alizadeh, In situ synthesis of vanadium carbide-copper nanocomposite by a modified mechanochemical combustion method, *Ceram. Int.* 42 (2016) 9371–9374.
- [17] C. Suryanarayana, Synthesis of nanocomposites by mechanical alloying, *J. Alloy. Compd.* 509 (2011) S229–S234.
- [18] B. Zhang, Z.Q. Li, Synthesis of vanadium carbide by mechanical alloying, *J. Alloy. Compd.* 392 (2005) 183–186.
- [19] E. Iglesia, J.E. Baumgartner, F.H. Ribeiro, M. Boudart, Bifunctional reactions of alkanes on tungsten carbides modified by chemisorbed oxygen, *J. Catal.* 131 (1991) 523–544.
- [20] F.H. Ribeiro, R.A.D. Betta, M. Boudart, J. Baumgartner, E. Iglesia, Reactions of neopentane, methylcyclohexane, and 3,3-dimethylpentane on tungsten carbides: the effect of surface oxygen on reaction pathways, *J. Catal.* 130 (1991) 86–105.
- [21] J.S. Lee, L. Volpe, F.H. Ribeiro, M. Boudart, Molybdenum carbide catalysts: II. Topotactic synthesis of unsupported powders, *J. Catal.* 112 (1988) 44–53.
- [22] S.T. Oyama, J.C. Schlatter, J.E. Metcalfe III, J.M. Lambert Jr., Preparation and characterization of early transition metal carbides and nitrides, *Ind. Eng. Chem. Res.* 27 (1988) 1639–1648.
- [23] Calka, W.A. Kaczmarek, The effect of milling conditions on the formation of nanostructures: synthesis of vanadium carbides, *Scr. Metall. Mater.* 26 (1992) 249–253.
- [24] R. Venugopalan, D. Sathiyamoorthy, Investigation through factorial design on novel method of preparing vanadium carbide using carbon during aluminothermic reduction, *J. Mater. Process. Technol.* 176 (2006) 133–139.
- [25] I. Nikolaenko, A. Krasovskaya, N. Kedim, G. Shveikin, Synthesis of ultrafine powder of vanadium carbide V8C7 by microwave heating, *Int. J. Mater. Res. (Former. Z. Met.)* 106 (2015) 10.
- [26] M. Mahajan, K. Singh, O.P. Pandey, Synthesis and analysis of high surface area vanadium carbide nanoparticles, *Adv. Mater. Res.* 585 (2012) 95–99.
- [27] M. Mahajan, K. Singh, O.P. Pandey, Synthesis of vanadium carbide nanoparticles by thermal decomposition of the Precursor, in: *Proceeding of International Conference on Recent Trends in Applied Physics and Material Science*, AIP Conf. Proc. 1536, 2013, pp. 271–272. (<http://dx.doi.org/10.1063/1.4810205>).
- [28] F. Liu, Y. Yao, H. Zhang, Y. Kang, G. Yin, Z. Huang, X. Liao, X. Liang, Synthesis and characterization of vanadium carbide nanoparticles by thermal refluxing-derived precursors, *J. Mater. Sci.* 46 (2011) 3693–3697.
- [29] Z. Zhao, Y. Liu, H. Cao, S. Gao, M. Tu, Synthesis of vanadium carbide nanopowders by thermal processing and their characterization, *Powder Technol.* 181 (2008) 31–35.
- [30] S.A. Hassanzadeh-Tabrizi, D. Davoodi, A.A. Beykzadeh, A. Chami, Fast synthesis of VC and V₂C nanopowders by mechanochemical combustion method, *Int. J. Refract. Met. Hard Mater.* 51 (2015) 1–5.
- [31] M. Hossein-Zadeh, M. Razavi, M. Safa, A. Abdollahi, O. Mirzaee, Synthesis and structural evolution of vanadium carbide in nano scale during mechanical alloying, *J. King Saud Univ. - Eng. Sci.* 28 (2016) 207–212.
- [32] M. Jalaly, M.Sh Bafghi, M. Tamizifar, F.J. Gotor, An investigation on the formation mechanism of nano ZrB₂ powder by a magnesiothermic reaction, *J. Alloy. Compd.* 588 (2014) 36–41.
- [33] C.R. Bowen, B. Derby, Selfpropagating high temperature synthesis of ceramic materials, *Br. Ceram. Trans.* 96 (1997) 25–31.
- [34] G.K. Williamson, W.H. Hall, X-ray broadening from field aluminium and wolfram, *Acta Metall.* 1 (1953) 22–31.
- [35] R. Ebrahimi-Kahrizangi, M. Kalani-Mahabadi, O. Torabi, An investigation on the mechanochemical behavior of the Ca-Cu₂O-WO₃ quaternary system to synthesize the Cu-WC nanocomposite powder, *Int. J. Refract. Met. Hard Mater.* 54 (2016) 75–81.
- [36] S.M. Salili, A. Ataie, Z. Sadighi, Effect of ball size and ball to powder ratio variation on crystallite size and formation of nanocrystalline materials in planetary ball mill, *Int. Congr. Adv. Appl. Phys. Mater. Sci.* AIP Conf. Proc. 1400 (2011) 127–130, <https://doi.org/10.1063/1.3663098>.
- [37] K. Tkacova, *Mechanical Activation of Minerals*, Elsevier, 1989.
- [38] C. Suryanarayana, Mechanical alloying and milling, *Progress. Mater. Sci.* 46 (2001) 1–184.
- [39] B.D. Cullity, *Elements of X Ray Diffraction*, Addison-Wesley Publishing Company, Inc, 1956.
- [40] J. Tomas, Mechanics of nanoparticle adhesion — a continuum approach, *Particles on surfaces 8: detection, Adhes. Remov.* (2003) 1–47.